
Q-attention: Enabling Efficient Learning for Vision-based Robotic Manipulation

Stephen James
Dyson Robotics Lab
Imperial College London
slj12@imperial.ac.uk

Andrew J. Davison
Dyson Robotics Lab
Imperial College London
a.davison@imperial.ac.uk

Abstract

Despite the success of reinforcement learning methods, they have yet to have their breakthrough moment when applied to a broad range of robotic manipulation tasks. This is partly due to the fact that reinforcement learning algorithms are notoriously difficult and time consuming to train, which is exacerbated when training from images rather than full-state inputs. As humans perform manipulation tasks, our eyes closely monitor every step of the process with our gaze focusing sequentially on the objects being manipulated. With this in mind, we present our Attention-driven Robotic Manipulation (ARM) algorithm, which is a general manipulation algorithm that can be applied to a range of sparse-rewarded tasks, given only a small number of demonstrations. ARM splits the complex task of manipulation into a 3 stage pipeline: (1) a Q-attention agent extracts interesting pixel locations from RGB and point cloud inputs, (2) a next-best pose agent that accepts crops from the Q-attention agent and outputs poses, and (3) a control agent that takes the goal pose and outputs joint actions. We show that current learning algorithms fail on a range of RLBench tasks, whilst ARM is successful. Videos and code found at: <https://sites.google.com/view/q-attention>.

1 Introduction

Despite their potential, continuous-control reinforcement learning (RL) algorithms have many flaws: they are notoriously data hungry, often fail with sparse rewards, and struggle with long-horizon tasks. The algorithms for both discrete and continuous RL are almost always evaluated on benchmarks that give shaped rewards [2, 33], a privilege that is not feasible for training real-world robotic application across a broad range of tasks. Motivated by the observation that humans focus their gaze close to objects being manipulated [20], we propose an Attention-driven Robotic Manipulation (ARM) algorithm that consists of a series of algorithm-agnostic components, that when combined, results in a method that is able to perform a range of challenging, sparsely-rewarded manipulation tasks.

Our algorithm operates through a pipeline of modules: our novel **Q-attention** module first extracts interesting pixel locations from RGB and point cloud inputs by treating images as an environment, and pixel locations as actions. Using the pixel locations we crop the RGB and point cloud inputs, significantly reducing input size, and feed this to a next-best-pose continuous-control agent that outputs 6D poses, which is trained with our novel **confidence-aware critic**. These goal poses are then used by a control algorithm that continuously outputs motor velocities.

As is common with sparsely-rewarded tasks, we improve initial exploration through the use of demonstrations. However, rather than simply inserting these directly into the replay buffer, we use a **keyframe discovery** strategy that chooses interesting keyframes along demonstration trajectories that is fundamental to training our Q-attention module. Rather than storing the transition from an initial state to a keyframe state, we use our **demo augmentation** method which also stores the

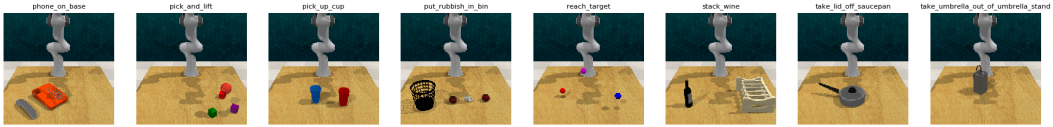


Figure 1: The 8 RLBench tasks used for evaluation. Current learning algorithms fail on all tasks, whilst our method succeeds within a modest number of steps. Note that the positions of objects are placed randomly at the beginning of each episode.

transition from intermediate points along a trajectories to the keyframe states; thus greatly increasing the proportion of initial demo transitions in the replay buffer.

All of these improvements result in an algorithm that starkly outperforms other state-of-the-art methods when evaluated on 8 RLBench [15] tasks (Figure 1) that range in difficulty. To summarise, we propose the following contributions: **(1)** An off-policy hard attention mechanism that is learned via Q-Learning, rather than the on-policy hard attention and soft attention that is commonly seen in the NLP and vision community. This work is the first to propose an off-policy hard attention module which is crucial because our demonstration data, by definition, is off-policy, and therefore renders existing hard attention approaches unusable for demonstration-driven RL. **(2)** A confidence-aware Q function that predicts pixel-wise Q values and confidence values, resulting in improved actor-critic stability. **(3)** A keyframe discovery strategy and demo augmentation method that go hand-in-hand to improve the utilisation of demonstrations in RL.

2 Related Work

The use of reinforcement learning (RL) is prevalent in many areas of robotics, including legged robots [18, 11], aerial vehicles [30], and manipulation tasks, such as pushing [5], peg insertion [22, 41, 21], throwing [7, 42], ball-in-cup [17], cloth manipulation [23], and grasping [16, 14]. Despite the abundance of work in this area, there has yet to be a general manipulation method that can tackle a range of challenging, sparsely-rewarded tasks without needing access to privileged simulation-only abilities (e.g. reset to demonstrations [25], asymmetric actor-critic [26], reward shaping [27], and auxiliary tasks [12]).

Crucial to our method is the proposed Q-attention. Soft and hard attention are prominent methods in both natural language processing (NLP) [1, 34, 4] and computer vision [39, 43]. Soft attention deterministically multiplies an attention map over the image feature map, whilst hard attention uses the attention map stochastically to sample one or a few features on the feature map (which is optimised by maximising an approximate variational lower bound or equivalently via (on-policy) REINFORCE [38]). Given that we perform non-differentiable cropping, our Q-attention is closest to hard attention, but with the distinction that we learn this in an off-policy way. This is key, as ‘traditional’ hard attention is unable to be used in an off-policy setting. We therefore see Q-attention as an off-policy hard attention. We elaborate further on these differences in Section 4.1.

Our proposed confidence-aware critic (used to train the next-best pose agent) takes its inspiration from the pose estimation community [37, 36]. There exists a small amount of work in estimating uncertainty with Q-learning in discrete domains [3, 10]; our work uses a continuous Q-function to predict both Q and confidence values for each pixel, which lead to improved stability when training, and is not used during action selection.

Our approach makes use of demonstrations, which has been applied in a number of works [35, 23, 16, 25], but while successful, they make limited use of the demonstrations and still can take many samples to converge. Rather than simply inserting these directly into the replay buffer, we instead make sure of our keyframe discovery and demo augmentation to maximise demonstration utility.

3 Background

The reinforcement learning paradigm assumes an agent interacting with an environment consisting of states $\mathbf{s} \in \mathcal{S}$, actions $\mathbf{a} \in \mathcal{A}$, and a reward function $R(\mathbf{s}_t, \mathbf{a}_t)$, where \mathbf{s}_t and \mathbf{a}_t are the state and action at time step t respectively. The goal of the agent is then to discover a policy π that results

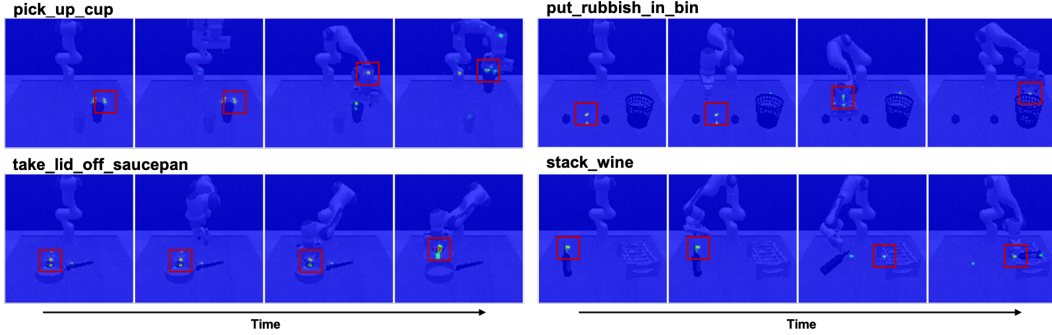


Figure 3: Visualising the Q values across 4 different points in time on 4 tasks. At each step, RGB and organised point cloud crops are made by extracting pixel locations that have the highest Q-value. Red squares indicated where the crop would be taken. We can see that as time progresses, the attention strength shifts depending on progress in the task; e.g. ‘stack_wine’ starts with high attention on the bottle, but after grasping, attention shifts to the wine rack. Videos of the Q-attention can be found on the project website.

All experiments are run in RLBench [15], a large-scale benchmark and learning environment for vision-guided manipulation built around CoppeliaSim [28] and PyRep [13]. At each time step, we extract an observation from the front-facing camera that consists of an RGB image \mathbf{b} and a depth image \mathbf{d} , along with proprioceptive information \mathbf{z} from the arm (consisting of end-effector pose and gripper open/close state). Using known camera intrinsics and extrinsics, we process each depth image to produce a point cloud \mathbf{p} (in world coordinates) projected from the view of the front-facing camera, producing a $(H \times W \times 3)$ ‘image’.

4.1 Q-attention

Motivated by the role of vision and eye movement in the control of human activities [20], we propose a Q-attention module that, given RGB and organised point cloud inputs, outputs 2D pixel locations of the next area of interest. With these pixel locations, we crop the RGB and organised point cloud inputs and thus drastically reduce the input size to the next stage of the pipeline. Our Q-attention is explicitly learned via Q-learning, where images are treated as the ‘environment’, and pixel locations are treated as the ‘actions’.

Given our Q-attention function Q_θ , we extract the coordinates of pixels with the highest value:

$$(\mathbf{x}_t, \mathbf{y}_t) = \underset{\mathbf{a}'}{\operatorname{argmax}} 2D Q_\theta(\mathbf{s}_t, \mathbf{a}'). \quad (4)$$

The parameters of the Q-attention are optimised by using stochastic gradient descent to minimise the loss:

$$J_Q(\theta) = \underset{(\mathbf{s}_t, \mathbf{a}_t, \mathbf{s}_{t+1}) \sim \mathcal{D}}{\mathbb{E}} [(\mathbf{r} + \gamma \max_{\mathbf{a}'} 2D Q_{\theta'}(\mathbf{s}_{t+1}, \mathbf{a}') - Q_\theta(\mathbf{s}_t, \mathbf{a}_t))^2 + \|Q\|], \quad (5)$$

where $\mathbf{s} = (\mathbf{b}, \mathbf{p})$, $Q_{\theta'}$ is the target Q-function, and $\|Q\|$ is an $L2$ loss on the per-pixel output of the Q function (which we call *Q regularisation*); in practice, we found that this leads to increased robustness against the common problem of overestimation of Q values. The Q-attention network follows a light-weight U-Net style architecture [29], which is summarised in Figure 2. Example per-pixel outputs of the Q-attention are shown in Figure 3. With the suggested coordinates from Q-attention, we perform a (16×16) crop on both the (128×128) RGB and organised point cloud data: $\mathbf{b}', \mathbf{p}' = \operatorname{crop}(\mathbf{b}, \mathbf{p}, (\mathbf{x}, \mathbf{y}))$.

Notably, there is no explicit reward for choosing a pixel, but instead an implicit reward that comes from the output of the method pipeline as a whole (i.e. the same reward signal is used to train both the Q-attention and the next-best pose agent). This leads to a cyclic dependency between the two agents: the lower-level next-best pose agent relies on receiving good crops from the Q-attention agent, whilst the Q-attention agent needs the next-best pose agent to perform well in order to get its implicit reward. This is where delicate handling of demonstrations is key, which we discuss in Section 4.4.

Algorithm 1 ARM

Initialise Q-attention network Q_θ , twin-critic networks $Q_{\rho_1}^\pi, Q_{\rho_2}^\pi$, and actor network π_ϕ with random parameters $\theta_1, \theta_2, \rho_1, \rho_2, \phi$
Initialise target networks $\theta' \leftarrow \theta, \rho'_1 \leftarrow \rho_1, \rho'_2 \leftarrow \rho_2$
Initialise replay buffer \mathcal{D} with demos and apply **keyframe discovery** and **demo augmentation**
for each iteration **do**
 for each environment step **do**
 $(\mathbf{b}_t, \mathbf{p}_t, \mathbf{z}_t) \leftarrow \mathbf{s}_t$
 $(x_t, y_t) \leftarrow \operatorname{argmax}_{2D_{\mathbf{a}'}} Q_\theta((\mathbf{b}_t, \mathbf{p}_t), \mathbf{a}')$ \triangleright Use Q-attention to get pixel coords
 $\mathbf{b}'_t, \mathbf{p}'_t \leftarrow \operatorname{crop}(\mathbf{b}_t, \mathbf{p}_t, (x_t, y_t))$
 $\mathbf{a}_t \sim \pi_\phi(\mathbf{a}_t | (\mathbf{b}'_t, \mathbf{p}'_t, \mathbf{z}_t))$ \triangleright Sample pose from the policy
 while target not reached **do**
 $v \leftarrow f(\mathbf{s}, \mathbf{a}_t)$ \triangleright Get joint velocities from control agent
 $\mathbf{s}_{t+1}, \mathbf{r} \leftarrow \operatorname{env.step}(v)$
 $\mathcal{D} \leftarrow \mathcal{D} \cup \{(\mathbf{s}_t, \mathbf{a}_t, \mathbf{r}, \mathbf{s}_{t+1}, (x_t, y_t))\}$ \triangleright Store the transition in the replay pool
 for each gradient step **do**
 $\theta \leftarrow \theta - \hat{\nabla}_\theta J_Q(\theta)$ \triangleright Update Q-attention parameters
 $\rho_i \leftarrow \rho_i - \hat{\nabla}_{\rho_i} J_{Q^\pi}(\rho_i)$ for $i \in \{1, 2\}$ \triangleright Update critic parameters
 $\phi \leftarrow \phi - \hat{\nabla}_\phi J_\pi(\phi)$ \triangleright Update policy weights
 $\theta' \leftarrow \tau\theta + (1 - \tau)\theta'$ \triangleright Update Q-attention target network weights
 $\rho'_i \leftarrow \tau\rho_i + (1 - \tau)\rho'_i$ for $i \in \{1, 2\}$ \triangleright Update critic target network weights

The module shares similar human-inspired motivation to the attention seen in NLP [1, 34, 4] and computer vision [39, 43], but differs in its formulation. Soft attention multiplies an attention map over the image feature map, whilst hard attention uses the attention map to sample one or a few features on the feature maps or inputs. Given that we perform non-differentiable cropping, we categorise our Q-attention as hard attention, but with 2 core differences: (1) most importantly, ‘traditional’ hard attention is optimised (on-policy) by maximising an approximate variational lower bound or equivalently via REINFORCE [38], whereas our Q-attention is trained off-policy; this is crucial because our demonstration data, by definition, is off-policy, and therefore renders existing hard attention approaches unusable for demonstration-driven RL. (2) The output of ‘traditional’ hard attention carry different semantics: a score function in the case of REINFORCE hard attention, and Q-value (expected cumulative reward of choosing that crop) in the case of Q-attention.

4.2 Next-best Pose Agent

Our next-best pose agent accepts cropped RGB \mathbf{b}' and organised point cloud \mathbf{p}' inputs, and outputs a 6D pose. This next-best pose agent is run every time the robot reaches the previously selected pose. We represent the 6D pose via a translation $\mathbf{e} \in \mathcal{R}^3$ and a unit quaternion $\mathbf{q} \in \mathcal{R}^4$, and restrict the w output of \mathbf{q} to a positive number, therefore restricting the network to output unique unit quaternions. The gripper action $\mathbf{h} \in \mathcal{R}^1$ lies between 0 and 1, which is then discretised to a binary open/close value. The combined action therefore is $\mathbf{a} = \{\mathbf{e}, \mathbf{q}, \mathbf{h}\}$.

To train this next-best pose agent, we use a modified version of SAC [8] where we modify the soft Q-function (Equation 1) to be a confidence-aware soft Q-function. Recent work in 6D pose estimation [37, 36] has seen the inclusion of a confidence score c with the pose prediction output for each dense-pixel. Inspired by this, we augment our Q function with a per-pixel confidence c_{ij} , where we output a confidence score for each Q-value prediction (resulting in a $(16 \times 16 \times 2)$ output). To achieve this, we weight the per-pixel Bellman loss with the per-pixel confidence, and add a confidence regularisation term:

$$J_{Q^\pi}(\rho) = \mathbb{E}_{(\mathbf{s}_t, \mathbf{a}_t, \mathbf{s}_{t+1}) \sim \mathcal{D}} [((\mathbf{r} + \gamma Q_{\rho'}^\pi(\mathbf{s}_{t+1}, \pi_\phi(\mathbf{s}_{t+1})) - \alpha \log \pi(\mathbf{a}_t | \mathbf{s}_t)) - Q_\rho^\pi(\mathbf{s}_t, \mathbf{a}_t))^2 c - w \log(c)], \quad (6)$$

where $\mathbf{s} = (\mathbf{b}', \mathbf{p}', \mathbf{z})$. With this, low confidence will result in a low Bellman error but would incur a high penalty from the second term, and vice versa. We use the Q value that has the highest

confidence when training the actor. As an aside, we also tried applying this confidence-aware method to the policy, though empirically we found no improvement. In practice we make use of the clipped double-Q trick [6], which takes the minimum Q-value between two Q networks, but have omitted in the equations for brevity. Finally, the actor’s policy parameters can be optimised by minimising the loss as defined in Equation 3.

4.3 Control Agent

Given the next-best pose suggestion from the previous stage, we give this to a goal-conditioned control function $f(s_t, g_t)$, which given state s_t and goal g_t , outputs motor velocities that drives the end-effector towards the goal. This function can take on many forms, but two noteworthy solutions would be either motion planning in combination with a feedback-control or a learnable policy trained with imitation/reinforcement learning. Given that the environmental dynamics are limited in the benchmark, we opted for the motion planning solution.

Given the target pose, we perform path planning using the SBL [31] planner within OMPL [32], and use Reflexxes Motion Library for on-line trajectory generation. If the target pose is out of reach, we terminate the episode and supply a reward of -1 . This path planning and trajectory generation is conveniently encapsulated by the ‘*ABS_EE_POSE_PLAN_WORLD_FRAME*’ action mode in RLbench [15].

4.4 Keyframe Discovery & Demo Augmentation

In this section, we outline how we maximise the utility of given demonstrations in order to complete sparsely reward tasks. We assume to have a teacher policy π^* (e.g. motion planners or human teleoperatives) that can generate trajectories consisting of a series of states and actions: $\tau = [(s_1, a_1), \dots, (s_T, a_T)]$. In this case, we assume that the demonstrations come from RLbench [15].

The **keyframe discovery** process iterates over each of the demo trajectories τ and runs each of the state-action pairs (s, a) through a function $K : \mathbb{R}^D \rightarrow \mathbb{B}$ which outputs a Boolean deciding if the given trajectory point should be treated as a keyframe. The keyframe function K could include a number of constraints. In practice we found that performing a disjunction over two simple conditions worked well; these included (1) change in gripper state (a common occurrence when something is grasped or released), and (2) velocities approaching near zero (a common occurrence when entering pre-grasp poses or entering a new phase of a task). It is likely that as tasks get more complex, K will inevitably need to become more sophisticated via learning or simply through more conditions, e.g. sudden changes in direction or joint velocity, large changes in pixel values, etc. Figure 5 shows RGB observations from the keyframe discovery process from 4 tasks.

At each keyframe, we use the known camera intrinsics and extrinsics to project the end-effector pose at state s_{t+1} into the image plane of state s_t , giving us pixel locations of the end-effector at the next keyframe. This stage is crucial to breaking the cyclic dependency (mentioned in Section 4.1) between the Q-attention and next-best pose agent, as these projected pixel coordinates act as optimal actions for the Q-attention agent.

Using this keyframe discovery method, each trajectory results in $N = \text{length}(\text{keyframes})$ transitions being stored into the replay buffer. To further increase the utility of demonstrations, we apply **demo augmentation** which stores the transition from an intermediate point along the trajectories to the keyframe states. Formally, for each point (s_t, a_t) along the trajectory starting from keyframe k_i , we calculate the transformation of the end-effector pose (taken from s_t) at time step t to the end-effector pose at the time step associated with keyframe k_{i+1} . This transformation can then be used as the action for the next-best pose agent. We repeat this process for every M th point along the

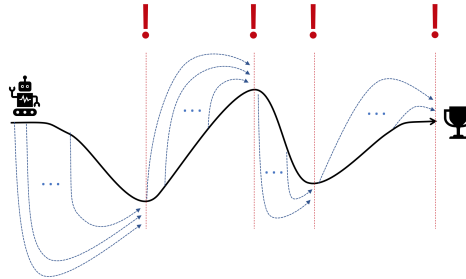


Figure 4: Keyframe discovery and demo augmentation, where the black line represents a trajectory, ‘!’ represents keyframes, and dashed blue lines represent the augmented transitions to the keyframes.

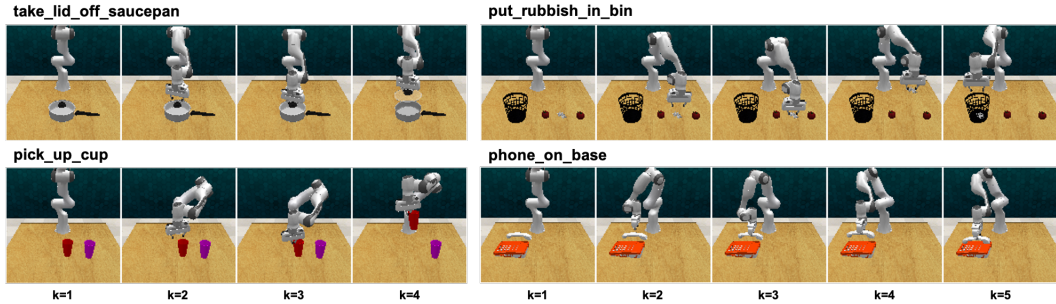


Figure 5: Visualising RGB observations of keyframes from the keyframe discovery process on 4 tasks. Here k is the keyframe number. Videos of the keyframe discovery can be found on the project website.

trajectory (which we set to $M = 5$). The keyframe discovery and demo augmentation is visualised in Figure 4.

5 Results

In this section, we aim to answer the following questions: (1) Are we able to successfully learn across a range of sparsely-rewarded manipulation tasks? (2) Which of our proposed components contribute the most to our success? (3) How sensitive is our method to the number of demonstrations and to the crop size? To answer these, we benchmark our approach using RL Bench [15]. Of the 100 tasks, we select 8 (shown in Figure 1) that we believe to be achievable from using only the front-facing camera. We leave tasks that require multiple cameras to future work. RL Bench was chosen due to its emphasis on vision-based manipulation benchmarking and because it gives access to a wide variety of tasks with demonstrations. Each task has a sparse reward of +1 which is given only on task completion, and 0 otherwise.

The first of our questions can be answered by attending to Figure 6. Our baselines include SAC [8] and behavioural cloning (BC). Other baselines that were tried include: DAC [19] (an improved, off-policy version of GAIL [9]) and TD3 [6]. DAC was omitted because we were unable to train this stably; note that we were unable to find work that has successfully trained DAC from images. TD3 was also omitted as this was less successful than SAC (as has been shown in prior work [8]). In addition, we also tried a modified, auto-encoder SAC [40], though this brought no additional performance; most likely because control-suite images can be reconstructed in a lossy manner without loss of performance, whereas in manipulation tasks, small details are needed (e.g. the handle on the saucepan). Code has been included in supplementary material which includes ARM, SAC, BC, DAC, and TD3.

The behaviour cloning and SAC baselines do not have our main contribution (Q-attention), but do have the keyframe discovery and demo augmentation. All methods receive the exact same 100 demonstration sequences, which are loaded into the replay buffer prior to training. The baseline agents are architecturally similar to the next-best pose agent, but with a few differences to account for missing Q-attention (and so receives the full, uncropped RGB and organised point cloud data). The SAC baseline does not have the confidence-aware critic, and so outputs single Q-values rather than per-pixel values. Specifically, the architecture uses the same RGB and point cloud fusion as shown in Figure 2. Feature maps from the shared representation are concatenated with the reshaped proprioceptive input and fed to both the actor and critic. The baseline actor uses 3 convolution layers (64 channels, 3×3 filter size, 2 stride), whose output feature maps are maxpooled and sent through 2 dense layers (64 nodes) and results in an action distribution output. The critic baseline uses 3 residual convolution blocks (128 channels, 3×3 filter size, 2 stride), whose output feature maps are maxpooled and sent through 2 dense layers (64 nodes) and results in a single Q-value output. All methods use the LeakyReLU activation, layer normalisation in the convolution layers, learning rate of 3×10^{-3} , soft target update of $\tau = 5^{-4}$, and a reward scaling of 100. Training and exploration were done asynchronously with a single agent (to emulate a real-world robot training scenario) that would continuously load checkpoints every 100 training steps.

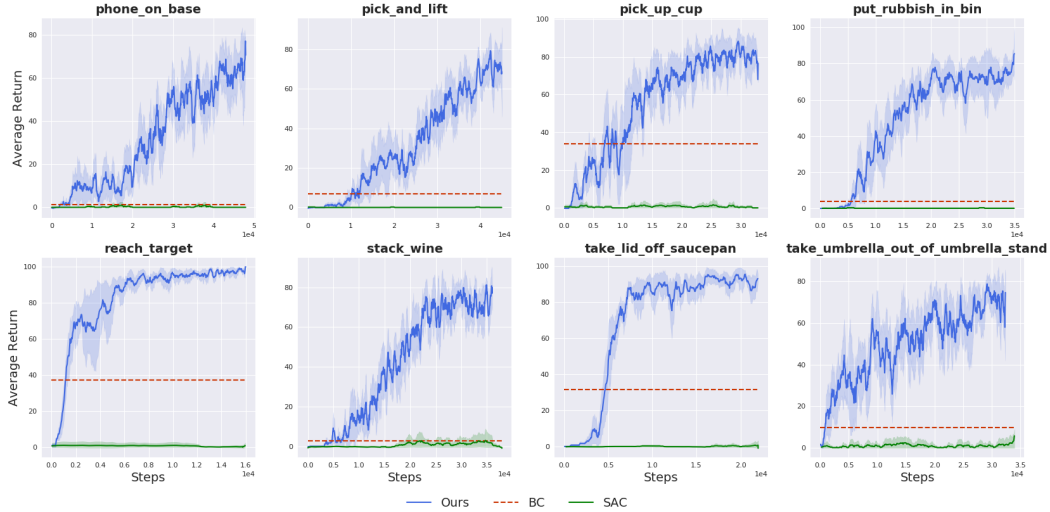
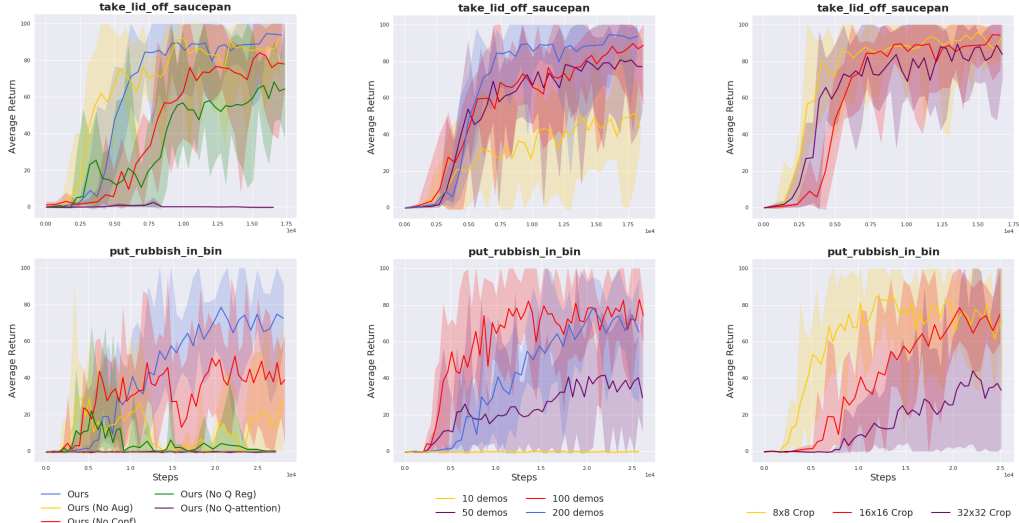


Figure 6: Learning curves for 8 RL Bench tasks. Methods include Ours (ARM), SAC [8], and behaviour cloning (BC). DAC [19] (an improved, off-policy version of GAIL [9]) was attempted as a baseline, however, we were unable to train this stably; note that we were unable to find work that has successfully trained DAC from images. TD3 was also trained, though this did not outperform SAC (as has been shown in prior work [8]). ARM uses the 3-stage pipeline (Q-attention, next-best pose, and control agent), while baselines use the 2-stage pipeline (next-best pose and control agent). All methods receive 100 demos which are stored in the replay buffer prior to training. Solid lines represent the average evaluation over 5 seeds, where the shaded regions represent the *min* and *max* values across those trials.

The results in Figure 6 show that baseline methods are unable to accomplish any RL Bench tasks, whilst our method is able to accomplish the tasks in a modest number of environment steps. We suggest that the reason why our results starkly outperform other methods is because of two key reasons that go hand-in-hand: (1) Reducing the input dimensionality through Q-attention that immensely reduces the burden on the (often difficult and unstable to train) continuous control algorithm; (2) Combining this with our keyframe discovery method that enables the Q-attention network to quickly converge and suggest meaningful points of interest to the next-best pose agent. We wish to stress that perhaps given enough training time some of these baseline methods may eventually start to succeed, however we found no evidence of this. To get SAC to successfully train on these tasks, it would need access to privileged simulation-only abilities (e.g. reset to demonstrations [25], asymmetric actor-critic [26], reward shaping [27], or auxiliary tasks [12]); this would then render the approach unusable for real-world training.

In Figure 7a, we perform an ablation study to evaluate which of the proposed components contribute the most to the success of our method. To perform this ablation, we chose 2 tasks of varying difficulty: ‘take_lid_off_saucepan’ and ‘put_rubbish_in_bin’. The ablation clearly shows that the Q-attention (combined with keyframe discovery) is crucial to achieving the tasks, whilst the demo augmentation, confidence-aware critic, and Q regularisation aid in overall stability and increase final performance. When swapping the Q-attention module with a soft attention [39] module, we found that performance was similar to that of the ‘vanilla’ baselines. This result is unsurprising, as soft attention is implicitly learned (i.e. without an explicit loss), whereas our Q-attention is explicitly learned via (off-policy) Q-learning, and so it can make greater use of the highly-informative keyframes given from the keyframe discovery process. Note that we cannot compare to ‘traditional’ hard attention because it requires on-policy training, as explained in Section 4.1.

Figure 7b shows how robust our method is when varying the number of demonstrations given. The results show that our method performs robustly, even when given 50% fewer demos, however as the task difficulty increase (from ‘take_lid_off_saucepan’ to ‘put_rubbish_in_bin’), the harmful effect of having less demonstrations is more severe. Our final set of experiments in Figure 7c shows how our method performs across varying crop sizes. As the task difficulty increases, the harmful effect of a



(a) Effect of removing components from our method. (b) Effect of number of demos on performance. (c) Effect of crop size on performance.

Figure 7: Ablation study across the easier ‘take_lid_off_saucepan’ task and harder ‘put_rubbish_in_bin’ task.

larger crop size becomes more prominent; suggesting that one of the key benefits of the Q-attention is to drastically reduce the input size to the next-best pose agent, making the RL optimisation much easier. It is clear that a trade-off must be made between choosing smaller crops to increase training size, and choosing larger crops to incorporate more of the surrounding area. We found that setting the crops at 16×16 across all tasks performed well.

6 Conclusion

We have presented our Attention-driven Robotic Manipulation (ARM) algorithm, which is a general manipulation algorithm that can be applied to a range of real-world sparsely-rewarded tasks. We validate our method on 8 RLbench tasks of varying difficulty, and show that many commonly used state-of-the-art methods catastrophically fail. We show that Q-attention (along with the keyframe discovery) is key to our success, whilst the confidence-aware critic and demo augmentation contribute to achieving high final performance.

Despite our experimental results, there are undoubtedly areas of weakness. The control agent (final agent in the pipeline) uses path planning and on-line trajectory generation, which for these tasks are adequate; however, this would need to be replaced with an alternative agent for tasks that have dynamic environments (e.g. moving target objects, moving obstacles, etc) or complex contact dynamics (e.g. peg-in-hole). We look to future work for swapping this with a goal-conditioned reinforcement learning policy, or similar. Another weakness is that we only evaluate on tasks that can be done with the front-facing camera; however we are keen to explore many of the other tasks RLbench has to offer by adapting the method to accommodate multiple camera inputs in future work. Finally, although our method does not use privileged simulation-only abilities, we believe it is still too sample inefficient to run in a reasonable amount of time (ideally less than 1 hour), and so we leave improving the sample efficiency even further for future work.

Acknowledgements

Research presented in this paper has been supported by Dyson Technology Ltd.

References

- [1] D. Bahdanau, K. Cho, and Y. Bengio. Neural machine translation by jointly learning to align and translate. *Intl. Conference on Learning Representations*, 2015.
- [2] G. Brockman, V. Cheung, L. Pettersson, J. Schneider, J. Schulman, J. Tang, and W. Zaremba. Openai gym. *arXiv preprint arXiv:1606.01540*, 2016.
- [3] W. R. Clements, B.-M. Robaglia, B. Van Delft, R. B. Slaoui, and S. Toth. Estimating risk and uncertainty in deep reinforcement learning. *arXiv preprint arXiv:1905.09638*, 2019.
- [4] J. Devlin, M.-W. Chang, K. Lee, and K. Toutanova. Bert: Pre-training of deep bidirectional transformers for language understanding. *arXiv preprint arXiv:1810.04805*, 2018.
- [5] C. Finn and S. Levine. Deep visual foresight for planning robot motion. In *IEEE Intl. Conference on Robotics and Automation*, pages 2786–2793. IEEE, 2017.
- [6] S. Fujimoto, H. Van Hoof, and D. Meger. Addressing function approximation error in actor-critic methods. *Intl. Conference on Machine Learning*, 2018.
- [7] A. Ghadirzadeh, A. Maki, D. Kragic, and M. Björkman. Deep predictive policy training using reinforcement learning. In *IEEE Intl. Conference on Intelligent Robots and Systems*, pages 2351–2358. IEEE, 2017.
- [8] T. Haarnoja, A. Zhou, K. Hartikainen, G. Tucker, S. Ha, J. Tan, V. Kumar, H. Zhu, A. Gupta, P. Abbeel, et al. Soft actor-critic algorithms and applications. *arXiv preprint arXiv:1812.05905*, 2018.
- [9] J. Ho and S. Ermon. Generative adversarial imitation learning. *Advances in Neural Information Processing Systems*, 2016.
- [10] C.-J. Hoel, K. Wolff, and L. Laine. Tactical decision-making in autonomous driving by reinforcement learning with uncertainty estimation. *arXiv preprint arXiv:2004.10439*, 2020.
- [11] J. Hwangbo, J. Lee, A. Dosovitskiy, D. Bellicoso, V. Tsounis, V. Koltun, and M. Hutter. Learning agile and dynamic motor skills for legged robots. *Science Robotics*, 4(26), 2019.
- [12] S. James, A. J. Davison, and E. Johns. Transferring end-to-end visuomotor control from simulation to real world for a multi-stage task. *Conference on Robot Learning*, 2017.
- [13] S. James, M. Freese, and A. J. Davison. Pyrep: Bringing v-rep to deep robot learning. *arXiv preprint arXiv:1906.11176*, 2019.
- [14] S. James, P. Wohlhart, M. Kalakrishnan, D. Kalashnikov, A. Irpan, J. Ibarz, S. Levine, R. Hadsell, and K. Bousmalis. Sim-to-real via sim-to-sim: Data-efficient robotic grasping via randomized-to-canonical adaptation networks. In *IEEE Conference on Computer Vision and Pattern Recognition*, pages 12627–12637, 2019.
- [15] S. James, Z. Ma, D. Rovick Arrojo, and A. J. Davison. RL Bench: The robot learning benchmark & learning environment. *IEEE Robotics and Automation Letters*, 2020.
- [16] D. Kalashnikov, A. Irpan, P. Pastor, J. Ibarz, A. Herzog, E. Jang, D. Quillen, E. Holly, M. Kalakrishnan, V. Vanhoucke, et al. Qt-opt: Scalable deep reinforcement learning for vision-based robotic manipulation. *Conference on Robot Learning*, 2018.
- [17] J. Kober and J. R. Peters. Policy search for motor primitives in robotics. In *Advances in Neural Information Processing Systems*, pages 849–856, 2009.
- [18] N. Kohl and P. Stone. Machine learning for fast quadrupedal locomotion. In *Association for the Advancement of Artificial Intelligence*, volume 4, pages 611–616, 2004.
- [19] I. Kostrikov, K. K. Agrawal, D. Dwibedi, S. Levine, and J. Tompson. Discriminator-actor-critic: Addressing sample inefficiency and reward bias in adversarial imitation learning. *Intl. Conference on Learning Representations*, 2019.

- [20] M. Land, N. Mennie, and J. Rusted. The roles of vision and eye movements in the control of activities of daily living. *Perception*, 28(11):1311–1328, 1999.
- [21] M. A. Lee, Y. Zhu, K. Srinivasan, P. Shah, S. Savarese, L. Fei-Fei, A. Garg, and J. Bohg. Making sense of vision and touch: Self-supervised learning of multimodal representations for contact-rich tasks. In *IEEE Intl. Conference on Robotics and Automation*, pages 8943–8950. IEEE, 2019.
- [22] S. Levine, C. Finn, T. Darrell, and P. Abbeel. End-to-end training of deep visuomotor policies. *Journal of Machine Learning Research*, 17(1):1334–1373, 2016.
- [23] J. Matas, S. James, and A. J. Davison. Sim-to-real reinforcement learning for deformable object manipulation. *Conference on Robot Learning*, 2018.
- [24] V. Mnih, K. Kavukcuoglu, D. Silver, A. A. Rusu, J. Veness, M. G. Bellemare, A. Graves, M. Riedmiller, A. K. Fidjeland, G. Ostrovski, et al. Human-level control through deep reinforcement learning. *nature*, 518(7540):529–533, 2015.
- [25] A. Nair, B. McGrew, M. Andrychowicz, W. Zaremba, and P. Abbeel. Overcoming exploration in reinforcement learning with demonstrations. In *IEEE Intl. Conference on Robotics and Automation*, pages 6292–6299. IEEE, 2018.
- [26] L. Pinto, M. Andrychowicz, P. Welinder, W. Zaremba, and P. Abbeel. Asymmetric actor critic for image-based robot learning. *Robotics: Science and Systems*, 2018.
- [27] A. Rajeswaran, V. Kumar, A. Gupta, G. Vezzani, J. Schulman, E. Todorov, and S. Levine. Learning complex dexterous manipulation with deep reinforcement learning and demonstrations. *Robotics: Science and Systems*, 2018.
- [28] E. Rohmer, S. P. Singh, and M. Freese. V-rep: A versatile and scalable robot simulation framework. In *IEEE Intl. Conference on Intelligent Robots and Systems*. IEEE, 2013.
- [29] O. Ronneberger, P. Fischer, and T. Brox. U-net: Convolutional networks for biomedical image segmentation. In *International Conference on Medical image computing and computer-assisted intervention*, pages 234–241. Springer, 2015.
- [30] F. Sadeghi and S. Levine. Cad2rl: Real single-image flight without a single real image. *Robotics: Science and Systems*, 2017.
- [31] G. Sánchez and J.-C. Latombe. A single-query bi-directional probabilistic roadmap planner with lazy collision checking. In *Robotics research*, pages 403–417. Springer, 2003.
- [32] I. A. Şucan, M. Moll, and L. E. Kavraki. The Open Motion Planning Library. *IEEE Robotics & Automation Magazine*, 19(4):72–82, December 2012. doi: 10.1109/MRA.2012.2205651. <https://ompl.kavrakilab.org>.
- [33] Y. Tassa, Y. Doron, A. Muldal, T. Erez, Y. Li, D. d. L. Casas, D. Budden, A. Abdolmaleki, J. Merel, A. Lefrancq, et al. Deepmind control suite. *arXiv preprint arXiv:1801.00690*, 2018.
- [34] A. Vaswani, N. Shazeer, N. Parmar, J. Uszkoreit, L. Jones, A. N. Gomez, Ł. Kaiser, and I. Polosukhin. Attention is all you need. In *Advances in Neural Information Processing Systems*, pages 5998–6008, 2017.
- [35] M. Vecerik, T. Hester, J. Scholz, F. Wang, O. Pietquin, B. Piot, N. Heess, T. Rothörl, T. Lampe, and M. Riedmiller. Leveraging demonstrations for deep reinforcement learning on robotics problems with sparse rewards. *arXiv preprint arXiv:1707.08817*, 2017.
- [36] K. Wada, E. Sucar, S. James, D. Lenton, and A. J. Davison. Morefusion: Multi-object reasoning for 6d pose estimation from volumetric fusion. In *IEEE Conference on Computer Vision and Pattern Recognition*, pages 14540–14549, 2020.
- [37] C. Wang, D. Xu, Y. Zhu, R. Martín-Martín, C. Lu, L. Fei-Fei, and S. Savarese. Densefusion: 6d object pose estimation by iterative dense fusion. In *IEEE Conference on Computer Vision and Pattern Recognition*, pages 3343–3352, 2019.

- [38] R. J. Williams. Simple statistical gradient-following algorithms for connectionist reinforcement learning. *Machine learning*, 8(3-4):229–256, 1992.
- [39] K. Xu, J. Ba, R. Kiros, K. Cho, A. Courville, R. Salakhudinov, R. Zemel, and Y. Bengio. Show, attend and tell: Neural image caption generation with visual attention. In *Intl. Conference on Machine Learning*, pages 2048–2057, 2015.
- [40] D. Yarats, A. Zhang, I. Kostrikov, B. Amos, J. Pineau, and R. Fergus. Improving sample efficiency in model-free reinforcement learning from images. *arXiv preprint arXiv:1910.01741*, 2019.
- [41] A. Zeng, S. Song, S. Welker, J. Lee, A. Rodriguez, and T. Funkhouser. Learning synergies between pushing and grasping with self-supervised deep reinforcement learning. In *IEEE Intl. Conference on Intelligent Robots and Systems*, pages 4238–4245. IEEE, 2018.
- [42] A. Zeng, S. Song, J. Lee, A. Rodriguez, and T. Funkhouser. Tossingbot: Learning to throw arbitrary objects with residual physics. *IEEE Transactions on Robotics*, 2020.
- [43] H. Zhang, I. Goodfellow, D. Metaxas, and A. Odena. Self-attention generative adversarial networks. In *Intl. Conference on Machine Learning*, pages 7354–7363, 2019.